Full vectorial BPM modeling of Index-Guiding Photonic Crystal Fibers and Couplers

Fabrizio Fogli, Luca Saccomandi and Paolo Bassi
Dipartimento di Elettronica Informatica e Sistemistica, DEIS, University of Bologna, Bologna, Italy
ffogli, lsaccomandi, pbassi@deis.unibo.it

http://www.deis.unibo.it

Gaetano Bellanca and Stefano Trillo
Dipartimento di Ingegneria, University of Ferrara, Ferrara, Italy
gbellanca, strillo@ing.unife.it

http://www.ing.unife.it

Abstract: A 3D full-vectorial Beam Propagation Method is successfully applied to compute both the propagation constants and the modal profiles in high-contrast silica-air index-guiding Photonic Crystal Fibers. The approach is intrinsically suited to investigate longitudinally varying structures or propagation and polarization effects, which are of practical interest for advanced optical applications. As an example we model a dual-core coupler, showing that efficient polarization preserving coupling can be expected.

OCIS codes: (060.2270) Fiber Characterization; (060.2310) Fiber Optics

References and links

1. J. C. Knight, J. Broeng, T. A. Birks, and P. St. J. Russel, "Single mode photonic band gap guidance of light in air," Science **282**, 1476-1478 (1998).
2. R. F. Cregan, B. J. Mangan J. C. Knight, T. A. Birks, P. St. J. Russel, P. J. Roberts, and D. C. Allan, "Single mode photonic band gap guidance of light in air," Science **285**, 1537-1539 (1999).
3. T.A. Birks, and P. St. J. Russel, "Endlessly single-mode photonic crystal fiber," Opt. Lett. **22**, 961-963 (1997).
4. D. Mogilevtsev, T. A. Birks, and P. St. J. Russel, "Group-velocity dispersion in photonic crystal fibers," Opt. Lett. **23**, 1662-1664 (1998).
5. J. C. Knight, T. A. Birks, P. St. J. Russel, and J. P. de Sandro, "Properties of photonic crystal fiber and the effective index model," J. Opt. Soc. Am. A **15**, 748-752 (1998).
6. E. Silvestre, M. V. Andrés, and P. Andrés, "Biorthonormal-basis method for the vector description of optical-fiber modes," IEEE J. Lightwave Tecnol. **23**, 923-928 (1998).
7. A. Ferrando, E. Silvestre, J. J. Miret, P. Andrés, and M. V. Andrés, "Full-vector analysis of a realistic photonic crystal fiber modes," Opt. Lett. **24**, 276-278 (1999).
8. A. Ferrando, E. Silvestre, J. J. Miret, P. Andrés, and M. V. Andrés, "Vector description of higher-order modes in photonic crystal fibers," J. Opt. Soc. Am. A **17**, 1333-1340 (2000).
9. T. M. Monro, D. J. Richardson, N. G. R. Broderick, and P. J. Bennet, "Modeling large air fraction holey optical fibers," IEEE J. Lightwave Tecnol. **18**, 50-56 (2000).
10. J. Broeng, S. E. Barkou, T. Sondergaard, and A. Bjarklev, "Analysis of air-guiding photonic bandgap fibers," Opt. Lett. **25**, 96-98 (2000).
11. M. J. Steel, T. P. White, C. M. de Sterke, R. C. McPhedran, and L. C. Botten, "Symmetry and degeneracy in microstructured optical fibers," Opt. Lett. **26**, 488-490 (2001).
12. X. Liu, C. Xu, W. Knox, J. K. Chandalia, B. J. Eggleton, S. G. Kosinski, and R. S. Windeler, "Soliton self-frequency shift in short tapered air-silica microstructure fiber," Opt. Lett. **26**, 358-400 (2001).
13. T. Sorensen, J. Broeng, A. Bjarklev, E. Knudsen, and S. E. Barkou Libori, "Macro-bending loss properties of photonic crystal fibre," Electron. Lett. **37**, 287-289 (2001).
14. B.J. Mangan, J.C. Knight, T. A. Birks, T.A. Roberts, P. St. J. Russel, and A. H. Greenaway, "Experimental study of dual-core photonic crystal fibre," Electron. Lett. **36**, 1358-1359 (2000).
15. M.D. Feit, and J. A. Fleck, "Computation of mode properties in optical fiber waveguides by a propagating beam method," Appl. Opt. **19**, 1154-1164 (1980).

#39853 - $15.00 US Received December 13, 2001; Revised January 2, 2002

16. B. J. Eggleton, P. S. Westbrook, C. A. White, C. Kerbage, R. S. Windeler and G. L. Burdge, "Cladddding-mode-resonances in air-silica microstructure optical fibers," IEEE J. Lightwave Tecnol. **18**, 1084-1100 (2000).
17. C. E. Kerbage, B. J. Eggleton, P. S. Westbrook, R. S. Windeler, "Experimental and scalar beam propagation analysis of an air-silica microstructure fiber," Opt. Expr. **7**, 13-122 (2000).
18. F. Fogli, G. Bellanca, P. Bassi, I. Madden, and W. Johnstone, "Highly Efficient Full-Vectorial 3-D BPM Modeling of Fiber to Planar Waveguide Couplers," IEEE J. Lightwave Tecnol. **17**, 136-143 (1999).

1. Introduction

Fibers characterized by a transverse section with periodic geometry have increasing impact in today research and future applications. These fibers, conventionally known as microstructured or Photonic Crystal Fibers (PCFs), are usually realized from a regular stack of silica hollow tubes with properly included longitudinally-invariant defects. Specific choices of the geometry lead to two basic guiding mechanisms, so-called photonic band gap effect and modified total internal reflection, respectively [1-5]. In the former case, the PCFs are made by inserting an extra hole in a honeycomb structure or by means of a hollow core, and the light is guided mainly in the air-filled region provided that the perfect periodicity exhibits a band-gap effect at the operating wavelength. Conversely, the latter confinement mechanism is similar to that of common waveguide devices, where the field is trapped around a high-index defect (i.e., a filled hole) and decays in the surrounding region with lower average refractive index [4-10]. These waveguides are usually referred to as index-guiding PCFs or holey fibers, and have interesting modal and dispersion properties which make them attractive and quite different from standard silica fibers [3-5].

While the analysis of propagation characteristics of PCFs was initially carried out in the scalar limit (see, e.g., Ref. [5]), considerable efforts have been recently devoted to investigate the vectorial case [6-11]. Although computationally intensive, this is crucial to assess the true dispersive features of such complex inhomogeneous structures. To this end, modal expansions or variational methods can be efficiently employed only to deal with cylindrical (i.e., pure longitudinally-invariant) structures, while they do not account for propagation effects. Conversely, it is definitely important to study also cases in which the field varies longitudinally, as in tapers [12], bends [13] or couplers [14]. For these structures, the Beam Propagation Method (BPM) algorithm [15] is clearly the natural choice. Even in its scalar weak-guidance implementation [16-17], the BPM is able to describe intriguing features of PCFs, such as the observed grating-assisted resonance of high-order (leaky) cladding modes. However, in high-contrast index-guiding PCFs or band-gap PCFs, it is well known that the vectorial nature of the field begins to play a significant role [8-10]. In this paper, our aim is to show that the full vectorial BPM is well suited to compute correctly the dispersion curves and all the field component profiles of the guided modes, despite the large index difference of an air-silica PCF, evidencing its inherent flexibility and robustness. The algorithm is then applied to model, for the first time, the true propagation effect due to (vector) mode coupling. To this end we have chosen a dual-core (i.e., double defect) PCF coupler of the type of those experimentally tested in Ref. [14]. In this paper we specifically focus on structures belonging to the class of index-guiding PCFs.

2. Dispersion features of the modes

For the sake of brevity, we refer the reader to Ref. [18] for the details of our finite difference implementation of BPM with Perfectly Matched Layers (PML) boundary conditions used in the calculations.

First, in order to validate our BPM code, the propagation in a PCF structure described in Ref. [8] has been simulated. In this way, the output of our code could be directly compared with results already obtained in the literature by means of a completely different method.

#39853 - $15.00 US Received December 13, 2001; Revised January 2, 2002

The structure consists of an air-filled silica (n = 1.46) index-guiding PCF characterized by an hexagonal distribution of air holes of radius a = 0.6 μm and pitch Λ = 2.3 μm with a central silica-filled hole which represents a high index defect. A transverse window of 19 μm x 14.2 μm in the x and y direction respectively, surrounded by a 1 μm thick PML boundary, has been used in the simulations. The mesh for the finite-difference computation has been generated using a spatial sampling step Δx = Δy = Δz =0.1 μm

According to Refs. [11], this structure allows the propagation of two degenerate x and y polarized modes, identified as a fundamental doublet. The next higher-order modes can be grouped into four degenerate multiplets, two x-polarized and two y-polarized respectively. In the simulations, one polarization of the fundamental doublet and one of the higher-order multiplets, both x-polarized, have been excited separately by launching nonmodal linearly polarized real fields with appropriate transverse symmetry. In particular we have used either the standard gaussian or the antisymmetric input field distributions shown in Fig. 1 to excite the first and the higher-order mode, respectively (in the following, simply referred to as the fundamental and upper mode, respectively). With this input conditions, along the PCF, no significant coupling between the fundamental and the upper mode has been observed in any of the performed simulations.

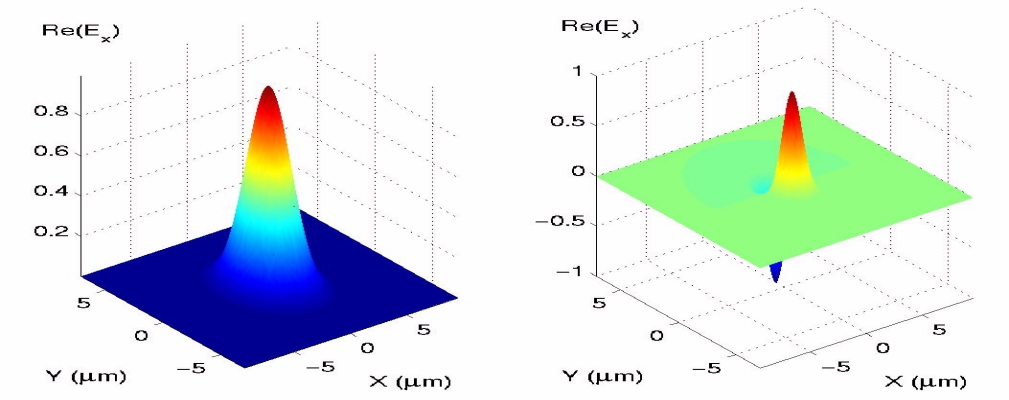

Fig. 1. Real part of the transverse profiles of the launched field (the imaginary parts are set to zero). Left frame: fundamental mode excitation. Right frame: upper mode excitation.

The modal effective index of the modes have been evaluated by the method described in Ref. [14], and the results are displayed in Fig. 2, where the BPM values (circles) are shown to be in very good agreement with those obtained in Ref. [8]. Moreover, the computed effective index of the upper mode crosses the analytically obtained one [8] close to cut-off (i.e., normalized frequency Λ/λ below 1.8), suggesting discrepancies between the two calculated dispersive behaviors. They can be explained by observing that, in the low frequency spectral region, the mode is no longer confined in the inner part of the structure. To cope with this problem, and increase the precision of the final results, the BPM would require a wider computational domain, in order to reduce the impact of the boundary conditions. However, similar constraints can be expected to hold also for the approach of Ref. [8]. Thus, in both cases, improving the precision demands only an increased computational effort.

As far as mode degeneracy is concerned [9-11], we have launched all the possible polarization states which compose the doublet and the multiplet, and found that maximum differences of effective index stabilize around 10^{-7} and 10^{-5} respectively, supporting the argument of degeneracy, within the estimated numerical precision of the method.

The three electric field components of the fundamental mode distribution are shown in Fig. 3 for a normalized frequency Λ/λ = 5. They have been obtained by propagating the input gaussian field of Fig. 1 (left frame), until it reaches a stable configuration over the transverse

#39853 - $15.00 US Received December 13, 2001; Revised January 2, 2002

section. The layout of the investigated structure is superimposed as well, for better readability of the results.

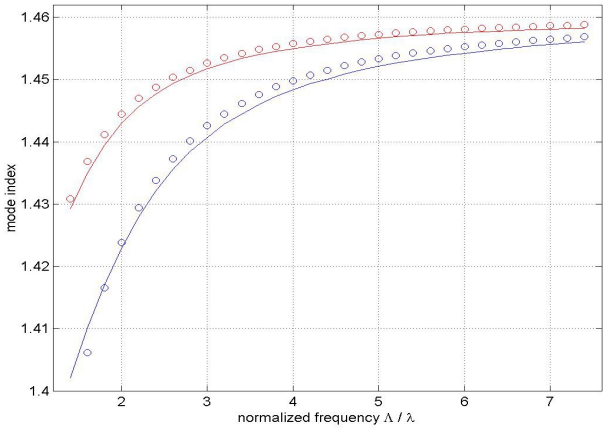

Fig. 2. Modal effective index vs. normalized frequency Λ/λ (λ varies from 300 to 1600 nm) for the fundamental mode and the next higher-order one of a PCF with a = 0.6 and Λ = 2.3 µm. The upper (red) and the lower (blue) curves refer to the fundamental and the higher order modes respectively. The open circles stand for BPM calculations whereas the solid lines show for comparison the data taken from Fig. 3 of Ref. [7].

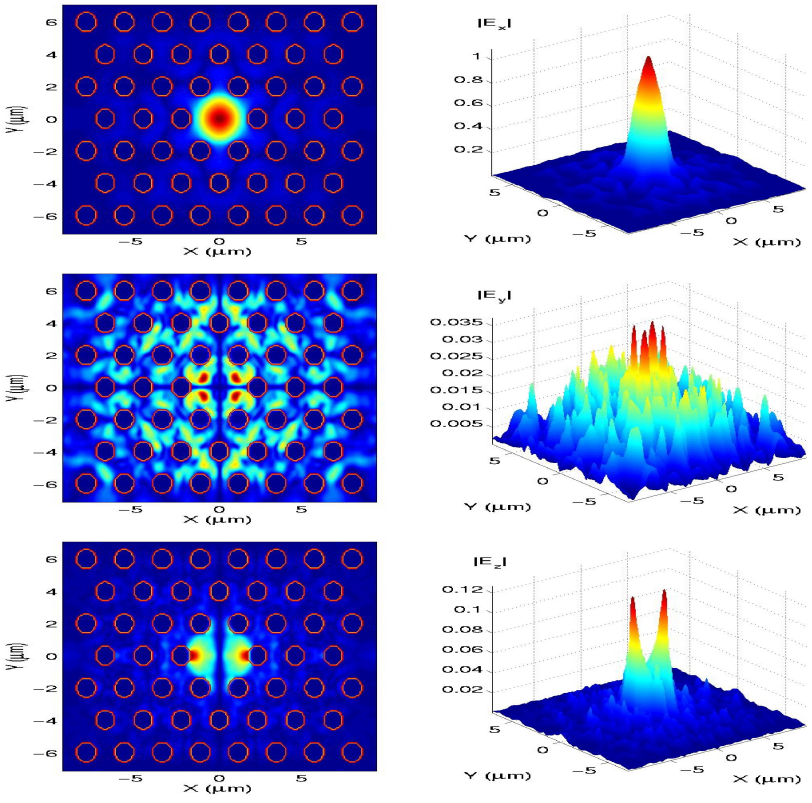

Fig. 3. Moduli of the *x*, *y* and *z* electric field components of the fundamental mode at the output section of the PCF for a normalized frequency Λ/λ = 5.

#39853 - $15.00 US Received December 13, 2001; Revised January 2, 2002

If both the *x*-polarized modes of the upper multiplet are excited by launching a 45 degrees oriented antisymmetric field distribution for the *x*-component, they reach the stable pattern shown in Fig. 4.

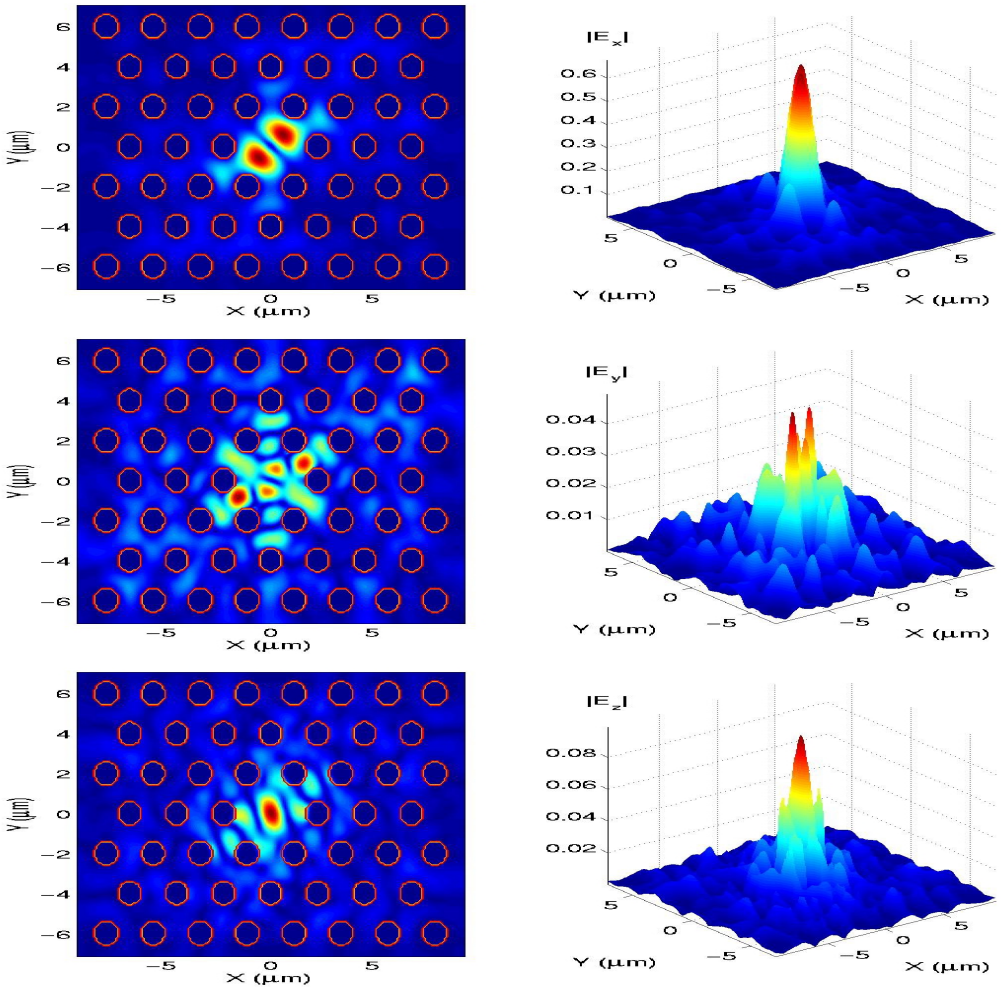

Fig. 4. Moduli of the x, y and z electric field components of the first upper mode at the output section of the fiber for a normalized frequency $\Lambda/\lambda = 5$.

Remarkably, the most effective *x*-directed field component, shown in Figs. 3 and 4, are very similar to the experimental near-field map presented in Ref. [5]. Moreover, the less significant one, directed along *y*, still exhibits a very regular pattern, despite its very low values, confirming the good reliability of our BPM algorithm.

3. The two-core structure

Once the BPM code has been successfully validated, we have applied it to study a dual-core PCF coupler, obtained by filling two holes of a single-mode PCF (a = 0.3 μm, Λ = 2.3 μm [8]) with an inter-core separation of 4.6 μm (twice the pitch). The *x*-polarized single fiber

#39853 - $15.00 US
Received December 13, 2001; Revised January 2, 2002

mode has been preliminarily calculated using the same procedure described before at a normalized frequency $\Lambda/\lambda = 2.7$. Then, this field has been launched along the left channel of the coupler, as shown in the left frame of Fig. 5 for the most significant field component.

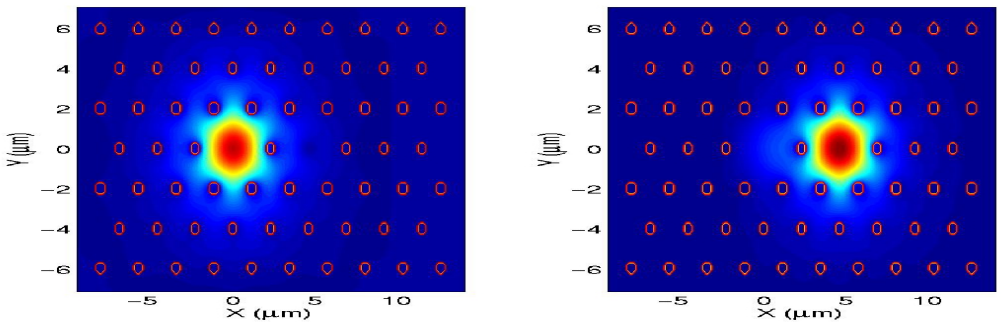

Fig. 5. Moduli of the x electric field components in the dual-core PCF Coupler for a normalized frequency $\Lambda/\lambda = 2.7$ overlaid with the investigated coupler geometry. Left: launched field in the starting section. Right: field distribution after a propagation distance of nearly 0.715 mm.

The right frame of Fig. 5 displays the same field component after a propagation distance of 0.7 mm. As shown, almost all the launched power is coupled into the right channel (around the right-end defect) of the coupler. Although our BPM code encompasses the possibility to have a dynamical evolution of the polarization, no significant polarization coupling is observed, meaning that the structure can operate in polarization preserving mode. The whole longitudinal field evolution along the structure has been recorded and post-processed to extract the coupling length of the device, which turns out to be L_c=0.7335 mm. Interestingly enough, by launching the y-polarization state of the doublet, we end up with the different value L_c=0.7505 mm. Such small difference in the coupling strength can be attributed to slight but significant differences in the x- and y-polarized field profiles of the doublet, which become detectable mainly at the air-silica interfaces around the main hole ring (surrounding the defect), where the field continuity plays a major role.

4. Conclusions

The 3D full-vectorial finite-difference BPM with PML boundary conditions has been proposed and validated to investigate the propagation properties of holey fibers. The method proves efficient in spite of the high-contrast of silica-air structures. The propagating fields and the relevant dispersion curves for both the fundamental and the higher-order modes have been successfully compared with previously published results obtained by means of completely different approaches. However, the method has greater flexibility as compared with mode-finder techniques, since it permits the study of propagation phenomena in PCF structures. To show this we have demonstrated that a dual-defect silica-air PCF can operate as a polarization preserving directional coupler. All the successfully performed tests are encouraging towards the applicability of this technique to study more complex directional coupling phenomena in longitudinally-invariant or adiabatically varying structures and devices such as those recently proposed [12-14].

Acknowledgements

Funding from CNR (MADESS II project) and MURST is gratefully acknowledged.

#39853 - $15.00 US Received December 13, 2001; Revised January 2, 2002